A Multi-Domain Thermal Model for Simulating Performance of High-Pressure Gerotor Pumps

Kai Ping Qwah, Ajinkya Pawar, Andrea Vacca, *Matthias Krug, *Michael Gunkel, *Christian Kretzer

Maha Fluid Power Research Center, Purdue University, 1500 Kepner Drive, 47905 Lafayette, IN, USA
E-mail: A. kqwah@purdue.edu, B. pawar10@purdue.edu, C. avacca@purdue.edu

*Thomas Magnete GmbH, Innomotion Park 3, 57562 Herdorf, Germany
E-mail: A. Matthias.Krug@thomas-magnete.com, B. Michael.Gunkel@thomas-magnete.com, C. Christian.Kretzer@thomas-magnete.com

Abstract

Gerotors are widely utilized as positive displacement units in low-to-medium pressure applications, such as automotive engine oil and fuel systems. Latest technological require higher operating pressure, and Gerotors are still a good candidate. Advanced simulation models can accelerate progresses in Gerotors. However, designing a Gerotor pump for high-pressure operation necessitates advanced modeling approaches that account for thermal effects, which are often overlooked in conventional isothermal models. Current methodologies, including 3D CFD, lumped parameter (LP), and coupled LP-lubricating interface models, fail to capture intricate temperature variations that influence frictional losses and leakages.

To address this gap, this paper presents a multi-domain numerical model that integrates thermal effects into the simulation of a gerotor pump operation. Utilizing a fully coupled LP-CFD-FEM framework, this approach is implemented via the proprietary Multics multi-physics simulation tool developed by the authors' research group. The model incorporates mass and energy conservation equations in the fluid domain using the LP methodology. Thermal Reynolds and energy equations are employed to simulate the lubricating interface, capturing thermoelastohydrodynamic (TEHL) effects, while solid components' heat transfer and thermal deformation are evaluated to establish a comprehensive coupling with lubricating interfaces and tooth space volumes (TSVs).

The proposed model provides detailed estimations of operating temperatures across pump's outlet, TSVs, lubricating interfaces, and solid components. Comparative analysis against isothermal models reveals significant differences in predicted frictional losses and leakages, emphasizing the critical role of thermal effects in gerotor pump performance. The results show a 5% rise in total efficiency prediction when thermal effects are considered compared to isothermal simulation. This work shows the importance of thermal considerations in a gerotor design for high pressure applications advancing the state of the art in gerotor pump modeling and simulation.

Keywords: Gerotor, coupled LP-lubricating interface, thermoelastohydrodynamic, frictional losses and leakages

1 Introduction

Gerotor pumps are commonly used in low-pressure fluid power and automotive applications. Their popular usage stems from its variety of benefits including low cost, compactness, robustness, and low noise when in operation. **Figure 1** illustrates a typical assembly for a Gerotor unit, which comprises of an inner gear, outer gear, shaft, casing, and lateral compensation plates.

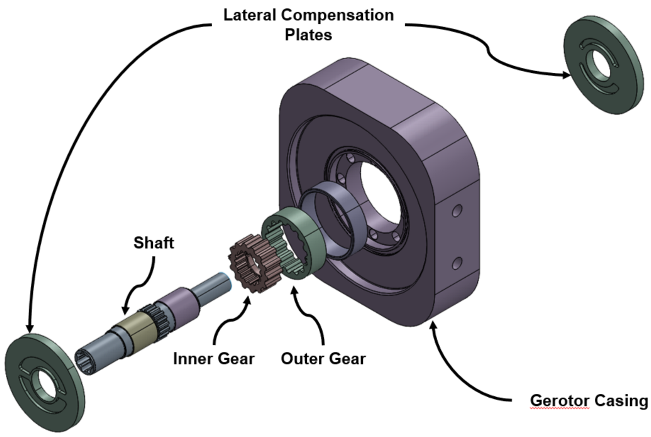

Figure 1: *Typical Gerotor Assembly.*

Figure 2 demonstrates the working of a Gerotor pump. The TSV expands as it connects to the low-pressure suction port, which allows for suction of flow into the TSV. Conversely, the TSV contracts as it connects to the high-pressure delivery port, which allows for delivery of flow from the TSV.

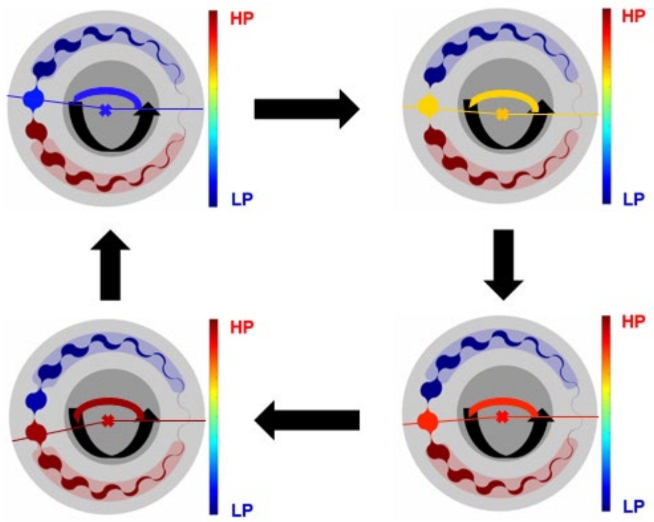

Figure 2: Principle of operation of a Gerotor.

A Gerotor pump has two primary lubricating interfaces as shown in **Figure 3**, which are the radial gap and the lateral gap.

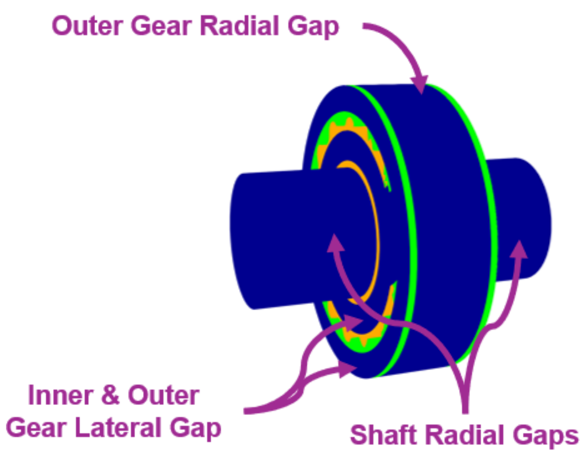

Figure 3: Lubricated interfaces of a Gerotor.

The outer radial gap supports the loads acting on the outer gear by virtue of hydrodynamic pressure developed in the oil. Similarly, the inner shaft radial gap supports the loads acting on the inner gear. The lateral gap is formed at the gear lateral side, and in common gerotor designs it is defined by the housing of the unit.

Gerotors are commonly used in the automotive industry, functioning as engine oil and fuel injection pumps. The pump operates under relatively low-pressure condition (p<30 bar) compared to the typical pressure levels experienced by other positive displacement machines (PDMs) ($p = 200\,bar$ to $300\,bar$). At high pressure applications, gerotors exhibit high inefficiencies due to pressure-driven leakages occurring at the lubricating interfaces as well as the clearances between moving components. Additionally, lubricating interfaces must be designed to support higher loads. Mixed or boundary lubrication can occur at higher pressures resulting in asperity contact which leads to high amounts of frictional shearing and wear on these surfaces.

To address excessive leakages at the lateral gap, a compensation mechanism in the form of thrust plates can be used [1]. Such mechanism is not common for Gerotors, but it is widely used in gear type Positive Displacement Machines [PDMs] such as external or internal gear machines. The lateral plate compensation design is a challenging aspect as the gear side loads can vary with operating speeds, with undercompensated designs showing higher leakages, while over-compensation can lead to higher frictional losses. The linear and angular micro-motion as well as deformation of compensating plates play a critical role in the overall power losses at lateral gap interface especially at high pressures. Recent developments in simulation models address these challenges by considering physical aspects of micro-motion and body deformation while modeling the lubricating interface performance and estimate power losses in pressure compensated designs. Thiagarajan et al. used a coupled LP-tribological model pressure-compensated design in an external gear machine (EGM) pump comprised of lateral bushings to analyze the designs of symmetric [2] as well as an asymmetric axial balancing configuration [3].

Pippes eta al. [4] studied the lubricating interfaces of crescent-type internal gear pump (CIGP) involved in compensation dynamic, which demonstrate the importance of compensation methods in controlling the flow leakages while ensuring an acceptable level of frictional losses. Pan et al. [5] proposed a model-based total efficiency prediction approach for a compensated CIGPs to study the energy losses within the unit and provide a solid foundation for predicting total efficiency for a compensated CIGP unit. However, there are various limitations with the above study, including the isothermal assumption and the neglection of deformation.

Examining the studies of compensated EGP and IGP highlights the importance of developing more accurate models to mirror the performances of actual units and demonstrate more accurately the volumetric efficiencies gained from a pressure-compensated unit in reference to an uncompensated unit.

Notable past efforts have engaged in modelling the fluid dynamic behavior of Gerotor units using LP or CFD approach. The first method to account for clearances between gears and subsequently the effects of fluid leakages as well as fluid compressibility effects was the lumped parameter model developed by Manco et al. [6], where the fluid volume is divided into lumped chambers and flow connections. Gamez et al. [7] proposed a leakage model in a 3-D CFD simulation which establishes a new boundary condition of a virtual wall to allow for simulation of the teeth contact at the interteeth radial clearance. Castilla et al. [8] introduced a novel methodology to achieve more realistic simulation of flow through channels and clearances of a new-born mini Gerotor prototype pump using OPENFOAM. Altare and Rundo [9] presented an extensive study on a reference Gerotor unit using a CFD model through the commercial software PumpLinx (now Simerics) to study the incomplete filling in Gerotor pumps with an accompanying experimental validation to verify the reliability of the CFD code. Bae et al. [10] analyzed the internal flow characteristics in the optimized Gerotor generated using a commercial CFD code, ANSYS-CFX.

Despite the popularity of computational fluid dynamics (CFD) based methods, a major disadvantage of these methods, besides the computational cost arising from the refined discretization of the fluid domain to capture complex geometries of the gerotor teeth, is their inability to reflect contacts and micro-motions. The contact behaviors between the teeth strongly affect their torque efficiency. Radial micromotions of the rotor also play a relevant role in determining the tooth tip sealing ability of the rotors. Pellegri et al. [11, 12, 13] demonstrated a comparison between CFD and lumped parameter (LP) model able to predict rotor micro-motion, showing how the rotor position predicted by the lumped parameter model could allow a good match between the results of all the models compared to experiments. More recently, Mistry et al. [14] developed a fully coupled LP-lubricating interface model that utilizes LP approach within the TSVs, solves Reynolds equation for the lubricating interfaces, and elasto-hydrodynamic lubrication (EHL) for evaluation of contact points between the gears. However, these models were limited by the isothermal consideration of the unit and did not consider any compensation mechanism due to low operating pressures. Due to larger power losses in Gerotors operating efficiently at high operating pressures there will be significant thermal effects on the unit that could affect the load-carrying capacity of the fluid significantly, resulting in smaller film gap heights at the lubricating interfaces and consequently a larger shearing at these interfaces, which ultimately leads to higher frictional losses and leakages uncaptured in an isothermal model.

To address these concerns, there has been an increasingly strong focus towards the development of thermal interaction models to capture thermal effects in positive displacement units. The first non-isothermal fluid model was introduced by Ivantysynova et al. [15] which addressed the variation of fluid properties in the fluid film at the piston/cylinder interface of an axial piston pumps. Since then, multiple studies [16, 17] have been proposed for thermoelastohydrodynamic (TEHL) analysis of various lubricating interfaces in piston pumps. Recently, Mukherjee et al. [18] proposed a comprehensive fully coupled simulation comprising of the thermal lumped-parameter fluid dynamics, thermoelastohydrodynamic lubrication (TEHL) for all lubricating interfaces, as well as the heat transfer, body dynamics, and solid deformation across these interfaces and control volumes (CVs) and illustrated that most power losses associated with the PDM are dominated by the lubricating interfaces. Pawar et al. [19] extended this methodology for the case of an external gear pump simulation, to study increasingly complex isothermal simulation to thermal simulation considering pressure and thermal deformation of gears, bushing and housing and analyzing their overall behavior in terms of EGP performance of a commercial unit. This study revealed the significance of thermal effects in accurate estimation of power losses. Since previous studies focused upon low pressure gerotor applications where power losses and thermal effects are not significant, there has not yet been a fully coupled TEHL model developed for Gerotor units.

This paper proposes a novel fully coupled thermal model for Gerotor under high-pressure applications ($> 50\ bar$). Additionally, the reference unit is pressure compensated by means of a compensation plate which is treated as a floating body which can move and deform, adding a new complexity to the lateral gap interface simulation compared to previous studies on gerotor pump analysis. Considering the state-of-the-art isothermal, strongly coupled model from Mistry, Z. [14] as baseline, this study, extends it to account for the thermal effects on the outer gear journal bearing radial gap and gears lateral gaps, as well as evaluates thermal behaviors of TSVs and the solid components including inner and outer rotor, compensation plate and housing. The analysis of the lateral compensation plate considering body dynamics, pressure and thermal deformation is a novel contribution for the Gerotor pump simulation and will be crucial in a more accurate and reliable evaluation of the lateral film leakage and frictional losses.

The remaining parts of the paper will be comprised of three sections. Section 2 will describe the details behind the methodology behind the fluid-structure interaction (FSI) – thermal coupled modeling, including the overall structure of the model, pertinent fluid dynamics, lubricating interface and thermal-related equations, and a summary of the overall TEHL model. Section 3 describes the simulation operating conditions and provides insights into the comparison between an isothermal and a thermal simulation of a reference Gerotor unit. Section 4 summarizes the results and provides a conclusion to the overall work.

2 Fluid-Structure Interaction (FSI)-Thermal Coupled Modelling Methodology

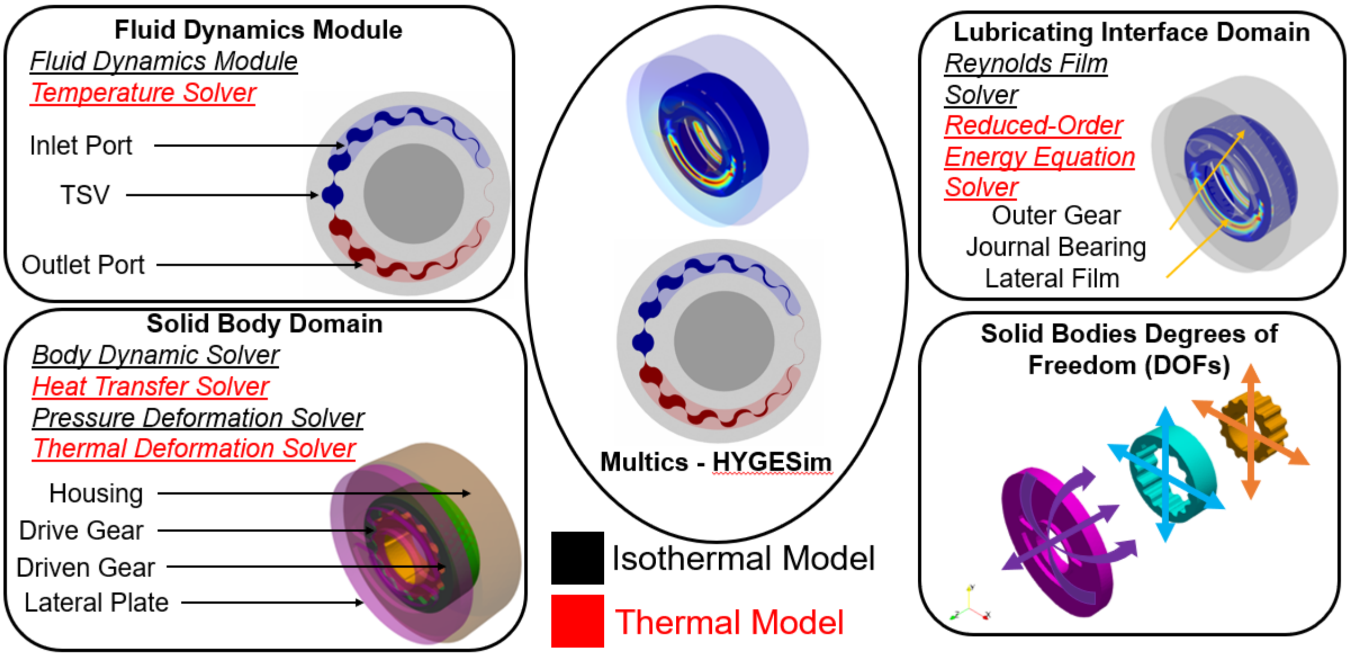

Figure 4: Gerotor Isothermal & Thermal Multi-Domain, Multi-Physics Simulation Model [Source: [14], [19]]

Figure 4 provides an overview of the Gerotor simulation model. The simulation model is comprised of the Preprocessor Module, as well as the multi-domain, multi-physics simulation tool consisting of fluid, solid body and lubricating interface domain solvers. CAD drawings are fed to the Geometric module which provides the input parameters to the multi-domain, multi-physics simulation tool, which includes the lumped parameter solution of the TSV fluid properties in the fluid domain, the evaluation of the behavior of the radial and lateral lubricating interfaces using the Reynolds film solver in the Lubricating Interface Domain, and the evaluation of the lateral compensation plate, inner and outer gear micro-motions through the Body Dynamics Solver as well as the analysis of deformation behaviors of these bodies through pressure deformation solver, Influence Matrix (IM), in the Solid Body Domain. Such tool is like what is presented in [14]. However, to include thermal effects, the tool has been extended to include thermal solvers, which are shown in **Figure 4** highlighted in red. Each domain in this thermal model will additionally include thermal solvers, such as Temperature Solver in the Fluid Domain, Reduced-Order Energy Equation Solver in the Lubricating Interface Domain, and Heat Transfer and Thermal Deformation Solver in the Solid Body Domain. A more detailed description for each solver will be provided in the following subsections.

Thermal simulation of Gerotor involves a fully coupled thermal lumped-parameter simulation of Gerotor. This simulation encompasses a variety of thermal effects on the unit. Firstly, a thermal lumped parameter model of the Gerotor is designed with the consideration of temperature variations during the suction and delivery of fluid within the TSVs due to convection effects at the teeth tips between TSVs and the conduction of heat from the inlet and outlet ports to the TSVs. Additionally, heat convection at the lateral films between compensation plate and Gerotor, and at the journal bearing film between the casing and Gerotor, as well as the heat conduction between these bodies are considered to provide a thermal coupling on the fluid and the solid bodies surrounding it. To evaluate the heat conduction and heat convection of the solid bodies (drive, driven gear, lateral plate, casing), a proper set of thermal boundary conditions are applied to the external surfaces of the bodies.

2.1 Fluid Domain

In the Fluid Domain, fluid dynamics solver is used to evaluate the fluid dynamics behavior by discretizing the pump domain into multiple CVs or TSVs. The choice of an LP model for this module allows for fast computations and permits easy interfacing with the other sub-modules. The layout of the connections can also be represented with the hydraulic schematic shown in **Figure 5**.

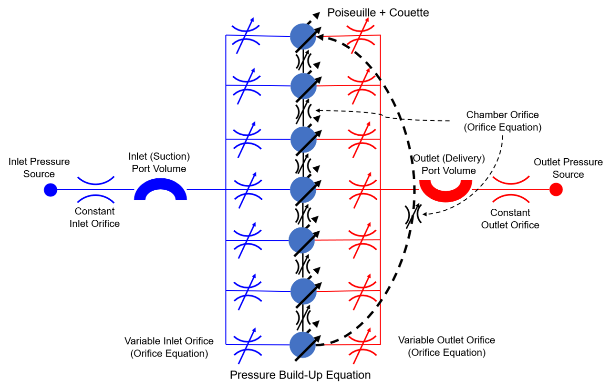

Figure 5: Representation of the control volumes (CV) and of the internal orifice connections.

This LP methodology is extended to a thermal pressure build-up equation Eq. (1) and lumped temperature equation (Eq. 2). These equations are solved for each control volume, or TSV, to compute the pressurization and temperature rise inside the pump. (i in Eq. (1) and Eq. (2) dictates the pressurization and temperature rise of each TSV).

Pressure Build-Up Equation:

$$\frac{\partial p_i}{\partial t} = \frac{K_T}{V}\left[\frac{1}{\rho}\sum \dot{m}_i - \frac{dV}{dt}\right] + K_T \alpha_p \frac{\partial T}{\partial t} \tag{1}$$

$\frac{K_T}{V}\frac{1}{\rho}\sum \dot{m}_i$ represents the time rate of change of fluid pressure due to incoming fluid time rate of volume flow, $-\frac{K_T}{V}\frac{dV}{dt}$ represents the time rate of change of fluid pressure due to outgoing fluid time rate of volume flow, and $K_T \alpha_p \frac{\partial T}{\partial t}$ represents the effects of fluid temperature build-up on the fluid pressure build-up.

Temperature Build-Up Equation:

$$\frac{\partial T_i}{\partial t} = \frac{1}{\rho c_p V}\left[\dot{Q} + \sum \dot{m}_i (h_i - h)\right] + \frac{\alpha_p T}{\rho c_p}\frac{\partial p}{\partial t} \tag{2}$$

$\frac{\dot{Q}}{\rho c_p V}$ represents the time rate of change in fluid temperature due to heat transfer across fluid, $\frac{\sum \dot{m}_i (h_i - h)}{\rho c_p V}$ represents the time rate of change in fluid temperature rise due to changes in fluid enthalpy, and $\frac{\alpha_p T}{\rho c_p}\frac{\partial p}{\partial t}$ represents the effects of fluid pressure build-up on the fluid temperature build-up.

The mass flow entering and leaving each TSVs ($\dot{m}_i$ in Eq. (1) & Eq. (2)) is evaluated using two different approaches: for the connection between each TSV and suction/delivery ports the orifice equation with variable flow coefficient α [15] has been used to account for both laminar and turbulent regimes. The mass flow rate equation is as follows:

$$\dot{m} = \frac{p_i - p_P}{|p_i - p_P|} \cdot \rho|_{p=\overline{p_{i,P}}} \cdot \alpha \cdot A_{i,P} \cdot \sqrt{\frac{2.(p_i - p_P)}{\rho|_{p=\overline{p_{i,P}}}}} \tag{3}$$

Here, the orifice flow coefficient α is a function of Reynolds Number (Re), as described in [20].

Each TSVs are connected via inner-teeth clearances known as tooth tip gap clearances, and these clearances are modelled as orifices with the assumption of laminar flow conditions. This is a reasonable assumption to model real flow conditions due to the microscopic scale in which the orifices are defined in. The modified Couette-Poiseuille equation derived by Rituraj et al. [21] is used to solve for the mass flow rate through the tooth tip gap clearances, which is dependent on geometrical gear properties such as equivalent radius of curvature, R_{eq} and gap height, h_t as well as the Couette flow term:

$$\dot{m} = \rho b \pi h_t \left[\frac{0.0456 b h_t^{2.4836} \Delta p}{\mu R_{eq}^{0.4836}} + \omega_{outer} r_{outer} - \omega_{inner} r_{inner}\right] \tag{4}$$

To solve for the equivalent radius of curvature R_{eq}, Eq. (5) is used:

$$\frac{1}{R_{eq}} = \frac{1}{R_1} + \frac{1}{R_2} \tag{5}$$

2.2 Lubricating Interface Domain

The lubricating films are modelled using the Reynolds Equation Solver. This solver solves for the pressure and density distribution in these film interfaces using the Universal Mixed Thermal Reynolds equation (Eq. 6).

$$\nabla_2 \cdot \left(\phi_P \left(\frac{K_T h^3}{12\mu}\nabla_2 \rho\right)\right) = \nabla_2 \cdot \left(\rho \vec{v}_m (\phi_R R_q) + \phi_c h\right) + \nabla_2 \cdot \left(\rho \phi_s R_q \left(\frac{v_t - v_b}{2}\right)\right) + \frac{\partial \rho(\phi_R R_q + \phi_c h)}{\partial t} - \nabla_2 \cdot \left(\phi_p \nabla_2 T \frac{K_T \alpha h^3}{12\mu}\right) \tag{6}$$

where

$\nabla_2 \cdot \left(\phi_P \left(\frac{K_T h^3}{12\mu}\nabla_2 \rho\right)\right)$: Poiseuille Term (Flow driven by pressure gradient)

$\nabla_2 \cdot \left(\rho \vec{v}_m (\phi_R R_q) + \phi_c h\right)$: Density Wedge Term (Flow due to change in fluid density with respect to position)

$\nabla_2 \cdot \left(\rho \phi_s R_q \left(\frac{v_t - v_b}{2}\right)\right)$: Squeeze Term (Flow due to changes in fluid film thickness with time)

$\frac{\partial \rho(\phi_R R_q + \phi_c h)}{\partial t}$: Local Expansion Term

$-\nabla_2 \cdot \left(\phi_p \nabla_2 T \frac{K_T \alpha h^3}{12\mu}\right)$: Fluid Volumetric Expansion due to Temperature Change

The use of ∇_2 refers to the gradient of variables in a 2-dimensional space (x-y).

2.2.1 Universal Mixed Thermal Reynolds Equation

Eq. (6) was derived initially by Ransegnola et al [22] to solve for both cavitated and non-cavitated regions on a lubricating interface through a single equation, but the equation was limited by simplifying assumption that the model is isothermal. Mukherjee et al. [23] modified this equation to include effects of thermal expansion of lubricant pressure.

An important property for a lubricating interface is the film gap height relative to the roughness profile of the bodies, which is crucial in determining the extent in which the film reaches a point of asperity contact with the bodies surrounding it. Lee and Ren [24] proposed an approach to estimate the contact forces based on the roughness profile of the bodies, which is done by relating the gap height information of the film to the contact pressure in the regime of asperity contact. This mixed lubrication modelling allows for evaluation of viscous and asperity friction, illustrated in Eq. (7) proposed by Manne et al. [20], resulting in a more accurate evaluation of power losses due to lubricating interfaces.

$$\vec{F}_{friction} = \int_{\Omega_S} \left(\frac{\vec{v}_c - \vec{v}_P}{h} + \frac{h\vec{\nabla}P}{2\mu_f} + \left(\mu_{Asp} p_{Cont} \vec{v}_D\right) \right) dA \quad (7)$$

where

$\int_{\Omega_S} \left(\frac{\vec{v}_c - \vec{v}_P}{h} + \frac{h\vec{\nabla}P}{2\mu_f} \right) dA$: Hydrodynamic Film Shear Force

$\int_{\Omega_S} \mu_{Asp} p_{Cont} \vec{v}_D \, dA$: Asperity Contact Shear Force

Another important attribute to the lubricating interface film gap height is the volumetric losses occurring between the film and its surrounding bodies. If these film gap heights are sufficiently large, a significant amount of volumetric flow losses could be incurred. To account for these losses, mass flow rate at the film boundaries is evaluated using Eq. (8), where s_i represents the boundary that defines the physical connection between a given lubricating interface and a lumped parameter volume.

$$\dot{m}_i = \int_{s_i} \left[-\phi_P \frac{K_T h^3}{12\mu_f} \vec{\nabla}\rho + \rho \vec{v}_m \left(\phi_R R_q + \phi_C h\right) + \rho \phi_S R_{eq} \left(\frac{\vec{v}_l - \vec{v}_b}{2} \right) \right] \cdot \vec{ds} \quad (8)$$

where

$\int_{s_i} -\phi_P \frac{K_T h^3}{12\mu_f} \vec{\nabla}\rho \cdot \vec{ds}$: Poiseuille Term

$\int_{s_i} \rho \vec{v}_m \left(\phi_R R_q + \phi_C h\right) \cdot \vec{ds}$: Couette Term

$\rho \phi_S R_q \left(\frac{\vec{v}_t - \vec{v}_b}{2} \right)$: Squeeze Term

2.2.2 Reduced Order Energy Equation

To determine the temperature distribution of a lubricating interface, a reduced order conservation of energy equation is used as shown in Eq. (9).

$$\frac{\partial(\rho c_p T)}{\partial t} + \nabla_2 \cdot \left(\rho c_p \vec{v}_f T\right) = \nabla_3 \cdot \left(\lambda_f \nabla_3 T\right) + \phi_D \quad (9)$$

where

$\frac{\partial(\rho c_p T)}{\partial t}$: Time Rate of Change in Heat

$\nabla_2 \cdot \left(\rho c_p \vec{v}_f T\right)$: Heat Convection Term

$\nabla_3 \cdot \left(\lambda_f \nabla_3 T\right)$: Heat Diffusion Term

ϕ_D: Heat Dissipation Term

Velocity in the convection term represents the fluid velocity field resulting from a combination of Couette and Poiseuille effects, as illustrated in Eq. (10).

$$\vec{v}_f = \phi_C \left(\vec{v}_b + (\vec{v}_t - \vec{v}_b) \frac{z}{h} \right) + \frac{\phi_P}{2\mu_f} (z^2 - zh) \vec{\nabla} p \quad (10)$$

$\phi_C \left(\vec{v}_b + (\vec{v}_t - \vec{v}_b) \frac{z}{h} \right)$: Couette Term

$\frac{\phi_P}{2\mu_f} (z^2 - zh) \vec{\nabla} p$: Poiseuille Term

Eq. (9) is converted into 2D Eq. (11) using the approach proposed by Mukherjee et al. [23] based on the Lobatto Point Collocation Method (LPCM) [25, 26] which considers a polynomial approximation of the temperature distribution across the film thickness.

$$\{C\} \frac{\partial\left(\rho c_p \{\hat{T}_k\}\right)}{\partial t} + \{C\} \nabla_2 \cdot \left(\rho c_p \vec{v}_f \{\hat{T}_k\}\right) = \{C\} \cdot \nabla_2 \cdot \left(\lambda_f \nabla_2 \{\hat{T}_k\}\right) + \frac{4\lambda_f}{h^2} \{E\}\{\hat{T}_k\} + \phi_D \quad (11)$$

$\{C\} \frac{\partial\left(\rho c_p \{\hat{T}_k\}\right)}{\partial t}$: LPCM-Modified Poiseuille Term

$\{C\} \nabla_2 \cdot \left(\rho c_p \vec{v}_f \{\hat{T}_k\}\right)$: LPCM-Modified Heat Convection Term

$\{C\} \cdot \nabla_2 \cdot \left(\lambda_f \nabla_2 \{\hat{T}_k\}\right) + \frac{4\lambda_f}{h^2} \{E\}\{\hat{T}_k\}$: LPCM-Modified Heat Diffusion Term

ϕ_D: LPCM-Modified Heat Dissipation Term

Heat dissipation denoted by ϕ_D arises due to viscous and asperity contact friction losses as shown in Eq. (12), and results from the double inner product of the shear stress tensor $[\tau]$ and the fluid velocity gradient $\nabla \cdot \vec{v}_f$

$$\phi_D = [\tau] : \nabla \cdot \vec{v}_f + \frac{dA}{dV} \left(\mu_{Asp} p_{Cont} |\vec{v}_t - \vec{v}_b| \right) \quad (12)$$

where

$[\tau] : \nabla \cdot \vec{v}_f$: Viscous Dissipation Term

$\frac{dA}{dV} \left(\mu_{Asp} p_{Cont} |\vec{v}_t - \vec{v}_b| \right)$: Friction Dissipation Term

2.3 Solid Body Domain

As is illustrated in **Figure 8**, the solid body domain modelling consists of Body Dynamics Solver, Pressure Deformation Solver, Heat Transfer Solver, and Thermal Deformation Solver.

2.3.1 Rigid Body Domain

Body Dynamics Solver is used to study the allowable degrees of freedom (DOFs) of the floating bodies (i.e. inner gear, outer gear, lateral compensation plate). Linear and angular behavior of the rigid body motions are evaluated using Newton's 2nd Law. Loads acting on the bodies from pressures of all the TSVs and lubricating interfaces as well as the possible contact and frictional forces are considered when evaluating the motion of bodies. In the present work, these loads are evaluated for the inner gear, outer gear and the lateral compensation plate of the Gerotor unit. The position and motion evaluated by the body dynamics solver allows for accurate estimation of the behavior of lubricating interfaces as well as tooth-tip gap heights.

2.3.2 Elastic Pressure Deformation

Pressure Deformation Solver solves pressure deformation using a finite element method (FEM) under reference loading conditions and uses the influence matrix approach (Eq. (13)) to estimate the body deformation and its influence on the change in gap height at lubricating interfaces. The current work involves the influence matrix pressure deformation of the lateral compensation plate of the reference Gerotor unit. The influence matrix approach implements the use of inertia relief methodology to simulate an unconstrained lateral plate in a static analysis using inertial forces, a method that was similarly used by Pelosi, Ivantysynova et al. [16].

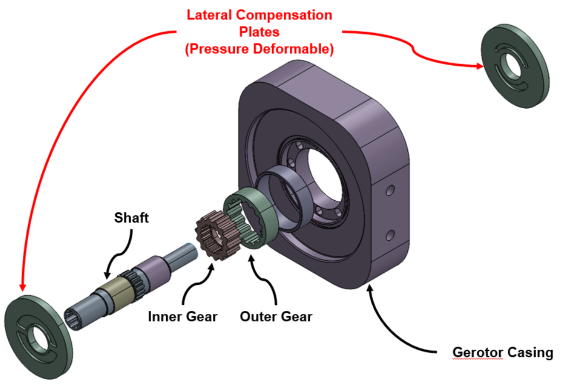

Figure 6: Reference Gerotor unit, highlighting lateral compensation plates as deforming bodies.

$$\Delta h_{eq} = [H]\{p\} \quad (13)$$

In the current work, pressure deformation is evaluated for the lateral compensation plate of the Gerotor to study the effects of deformation on the behavior of the lateral film, as is shown in **Figure 6**..

2.3.3 Heat Transfer

Temperature distribution of solid bodies comprising of the gears, lateral compensation plate, and the casing of the Gerotor are determined by the Heat Transfer Solver. The current work utilizes a 3-dimensional steady state heat transfer equation analysis, as shown in Eq. (15), to estimate the temperatures of all solid bodies in the Solid Body Domain. As discussed by Mukherjee et al. [23], the thermal transience of solid components is much slower than the thermal transience of fluid film lubricating interfaces physically due to the much higher heat capacity of the solid components and therefore modeling it is computationally expensive. To overcome this issue, a steady-state heat transfer equation is used for temperature estimation.

$$\nabla \cdot (\lambda_S \nabla_3 T) = 0 \quad (15)$$

Eq. (15) is a standard heat conduction equation between solid bodies. Eq. (15) is solved using FEM on a linear tetrahedral mesh for characteristic time periods. In the present simulation, the solid bodies of the Gerotor are evaluated for every revolution. This can be perceived as a limitation to Eq. (15), but it is sufficiently accurate in the evaluation of solid body temperatures, since the rate of change in temperatures of solid bodies are much lower than that in the fluid films between these bodies. Solid components temperature is then determined using Eq. (16):

$$T^n = T^{n-1} + \alpha_{relax}(T^n_{sol} - T^{n-1}) \quad (16)$$

where

T^i: Current Temperatures of Solid Bodies

T^{i-1}: Previous Temperatures of Solid Bodies

T^n_{sol}: Current solution of Eq. (15)

α_{relax}: Relaxation Factor ($\alpha_{relax} < 1$).

As the simulation approaches convergence or steady-state solution, temperature difference term, $(T^n_{sol} - T^{n-1})$ in Eq. (16) approaches zero. Relaxation factor α_{relax} is instrumental to couple the steady-state heat transfer equation with other transient system of equations to ensure a smooth transition and avoid sudden temperature gradients in the boundary conditions for reduced-order energy equation (Eq. (11)) in the fluid domain.

2.3.4 Thermal Deformation

Temperature rises occurring due to power losses in a Gerotor unit result in thermal deformation of solid components. In general, solid component deformation, termed thermal warping, can prominently affect the gap height distribution of the lubricating film interfaces in all PDMs, which results in TEHL effects. Thermal deformation is modelled by evaluating the thermal strain using a steady-state solid temperature distribution, evaluated from the steady-state heat transfer equation (Eq. (17))

$$\epsilon_T = \alpha_s \Delta T \begin{bmatrix} 1 \\ 1 \\ 1 \end{bmatrix} \quad (17)$$

and then relaxing this distribution to find the thermal stress and body deformations, solved using Eqs. (18) to (20).

$$\sigma = 2\mu_L \epsilon + \lambda_L \epsilon_T I \quad (18)$$

$$\nabla_3 \cdot \sigma + f = 0 \quad (19)$$

$$\mu_L = \frac{E}{2(1+\nu)}, \lambda_L = \frac{\nu E}{(1+\nu)(1-2\nu)} \quad (20)$$

3 Results

The reference Gerotor unit is simulated under 2 different operating conditions with the same operating speed of 1000 RPM and operating pressure ranging from an inlet pressure of 0 bar to an outlet pressure of 100 bar. ISOVG-46 is considered as the operating fluid with kinematic viscosity, ν at 40 °C. Nominal dimensions of the unit are considered for the simulations. The two different operating conditions are described as follows. The first case is an isothermal simulation conducted considering pressure deformation of the lateral plate. The second case is a thermal simulation with the same lateral plate considering both temperature and pressure deformations.

The novelty in these results is reflected in both the isothermal and thermal simulations. Isothermal simulation introduces a pressure-compensated lateral plate design under extreme operational conditions. Thermal simulations couples both the novelty of a lateral compensated Gerotor pump implementation with the thermal simulation of the model.

Figure 7 illustrates the film and mixed boundary conditions for the evaluation of lateral plate and casing temperatures.

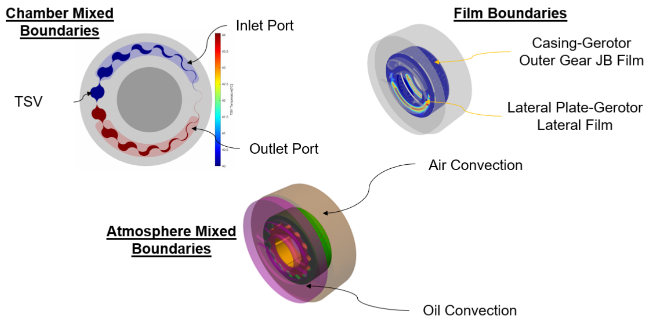

Figure 7: Film and Mixed Boundary Conditions for Lateral Plate and Casing temperature evaluation.

Table 1 shows the important parameters of the reference unit.

Table 1: Parameters of reference Gerotor

Gerotor Parameters	Values
Displacement	3.365 cc/rev
Gear Material	Low-Alloy Steel

3.1 Operational Settings of Isothermal & Thermal Simulation with Lateral Plate Pressure Deformation

Table 2 describes the operating conditions of the isothermal simulation of the unit.

Table 2: Operating Properties and Considerations for Isothermal Simulation

Operating Properties	Values
Shaft Speed	1000 RPM
Inlet Pressure	0 bar
Outlet Pressure	100 bar
Initial, Inlet & Outlet Temperatures	40 °C

Table 3 describes the operating conditions of the thermal simulation of the unit.

Table 3: Operating Properties and Considerations for Thermal Simulation

Operating Properties	Values
Shaft Speed	1000 RPM
Inlet Pressure	0 bar
Outlet Pressure	100 bar
Initial & Inlet Temperatures	40 °C
Outlet Temperature	45.8 °C

In a thermal simulation, TSV temperature follows a much longer transience than TSV pressure, and this is especially notable when thermal simulation is conducted with an outlet temperature set to inlet temperature. To accelerate this thermal transience, a separate thermal pure LP simulation is conducted to evaluate a steady-state outlet port temperature which is then used as the outlet port temperature. The steady-state temperature of 45.8 °C was evaluated after a total computational time of about 50 hours.

Additionally, a comparison of TSV pressures for both isothermal and thermal simulation is shown in **Figure 8**, which illustrates a similar pressure profile but with a slightly steeper pressurization in the thermal simulation, due to the influence of TSV temperature rise as it connects to the outlet port.

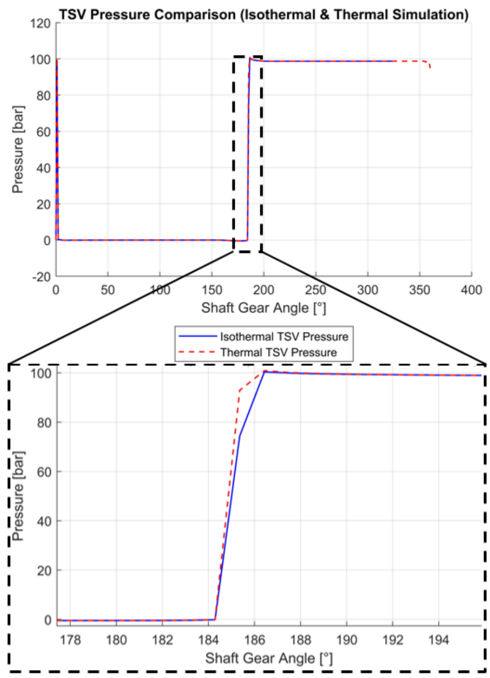

Figure 8: TSV Pressure Comparison for Isothermal & Thermal Simulation (top), highlighting also the steeper pressurization of thermal simulation (bottom).

Setting up thermal simulation requires a sufficiently accurate evaluation of the heat convection coefficient of various surfaces of the solid bodies. Zecchi [27] proposed an equation to approximate the heat flux associated with each region through viscous dissipation, as illustrated in (Eq. 21) below:

$$q \approx \frac{\mu h_{or}\left[\frac{\omega\left(R_{or,out} + R_{or,out}\right)}{2h_{or}}\right]^2}{2} \tag{21}$$

Where μ is the fluid viscosity, ω is the rotational speed, $R_{or_{out}}$ and $R_{or_{in}}$ are respectively the outer and inner radii of the surface and h_{or} is the fluid film thickness the heat flux associated with the region. In general, h_{or} represents the clearance existing in a particular region, such as the clearances within the lateral and outer gear journal bearing films.

Upon evaluating the heat flux, the convection coefficient is determined using the mixed boundary condition equation, shown below also by Zecchi [27]:

$$h \approx \frac{q}{(T_S - T_\infty)} \quad (22)$$

Where h is the heat convection coefficient associated with the heat exchange at the surface, T_S is the surface temperature, and T_∞ is the temperature of the fluid surrounding the surface.

$T_S - T_\infty$ is evaluated as the difference between the surface temperatures (40 °C) denoted by T_S and the fluid temperature (42.9 °C) denoted by T_∞.

Table 4 displays the heat convection coefficients that were considered for all the thermal boundary conditions using Eq. (22).

Table 4: Heat Convection Coefficients of Mixed Boundary Conditions

Mixed Boundary Conditions	**Heat Convection Coefficients [W/m^2/K]**
Tank Drain	348.5
Air	50
TSVs	2175.4
Outer Gear Journal Bearing	935.1
Inner Gear Lateral Film	418.7
Outer Gear Lateral Film	2130.1

3.2 Isothermal & Thermal Simulation with Lateral Plate Pressure Deformation Results

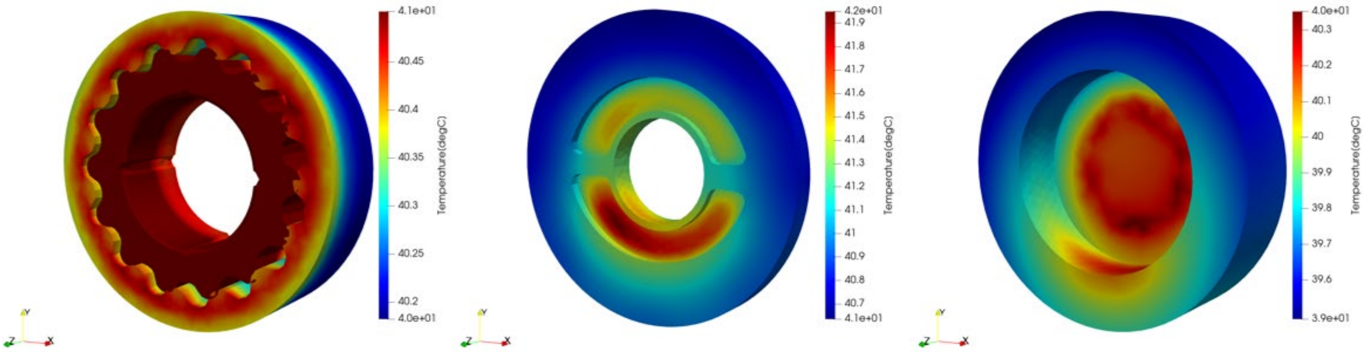

Figure 9: Gerotor (Left), Lateral Plate (Middle) & Casing (Right) Temperature Distribution.

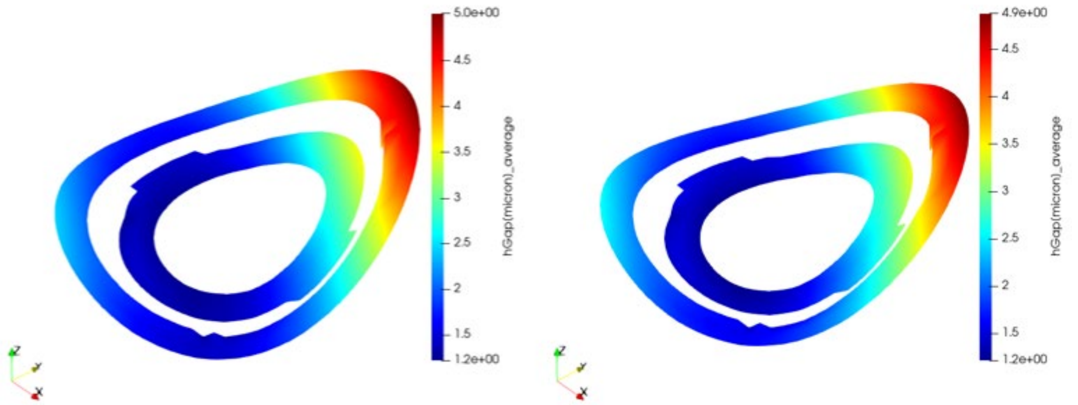

Figure 10: Isothermal (Left) & Thermal Simulation (Right) Time-Averaged Lateral Film Gap Height Comparison

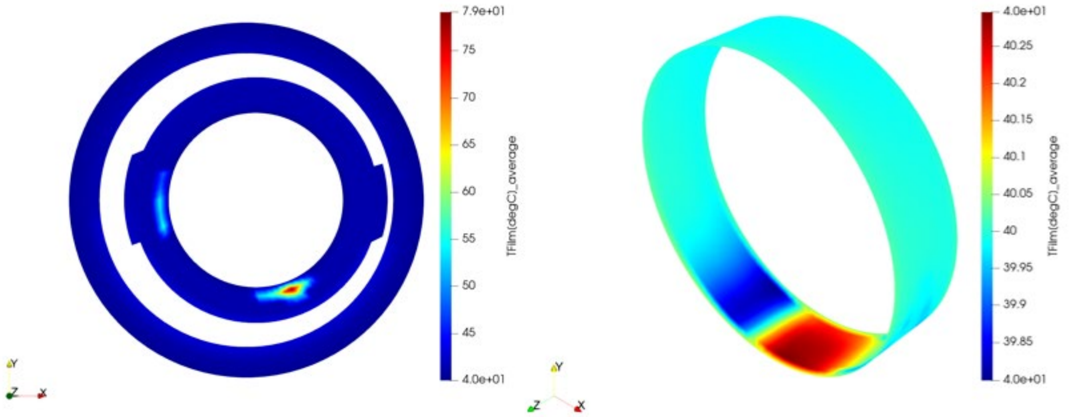

Figure 11: Lateral Film (Left) & Outer Gear Journal Bearing (Right) Time-Averaged Temperature Distribution

As can be observed from **Figure 9** and **Figure 11** heating spots are located where asperity contact occurs, and the temperature rise is much smaller in the solid bodies (40 °C to 42 °C) compared to the lateral film (40 °C to 79 °C).

Table 5 highlights the difference in the efficiencies and power loss percentage in both isothermal and thermal simulation. Power loss is evaluated by using the following equation:

$$\eta_{power\ loss} = \frac{Q_{outlet}\Delta p}{T_{shaft} + T_{inner} + T_{outer}} \cdot 100\ \% \qquad (22)$$

Table 5: Difference in Average Volumetric, Hydromechanical & Total Efficiencies between Isothermal and Thermal Simulations

Average Efficiency Properties	Difference between Isothermal & Thermal Simulation, $\eta_{thermal} - \eta_{isothermal}$
η_{vol}	+ 3.8 %
η_{hm}	+ 4.2 %
η_{total}	+ 5.3 %
P_{loss}	- 5.3 %

As is shown in **Table 5**, there is a slight increase in both the volumetric and hydromechanical efficiencies in the thermal model compared to the isothermal model. This can be attributed to difference in the volumetric losses across primarily the lateral film and the tooth tip leakages, as is illustrated in **Table 6**. Additionally, since it is also shown that the difference in the lateral film leakage loss is much higher than the tooth tip leakage loss, we can deduce that the largest contributor in the difference in the volumetric efficiency between an isothermal and thermal simulation is derived from the percentage differences in the lateral film leakage loss.

Table 6: Percentage Difference in Volumetric Loss between Isothermal and Thermal Simulation

Average Volumetric Loss Properties	Percentage Difference between Isothermal & Thermal Simulation, $\frac{Q_{loss,thermal} - Q_{loss,isothermal}}{Q_{loss,isothermal}}$
Lateral Film Leakage Loss	- 51.5 %
Tooth Tip Leakage Loss	- 1.1 %

Additionally, **Figure 10** shows that the overall gap height distribution shows a slightly larger region of more uniformly smaller gap heights from the thermal simulation. This is due to the temperature distribution of the film, as illustrated in **Figure 11**, which shows concentrated spots of high temperature on the film resulting in a reduction of fluid viscosity and consequently the load carrying capacity of the lateral film.

Additionally, **Table 7** demonstrates the much longer computational time required by thermal simulation compared to an isothermal simulation, which creates a trade-off between the higher degree of model accuracy offered and the more expensive computation required by thermal simulation.

Table 7: Average Computational Time for Isothermal and Thermal Simulation

Cases	Simulation Time
Isothermal (Lateral Plate Deformation)	3-4 days
Thermal (Lateral Plate Deformation + Thermal)	7-9 days

4 Conclusion

Current study serves to present a comparative analysis between an isothermal and thermal simulation model of a Gerotor unit, and to also emphasize the effects of deformation of the lateral pressure compensation plate as well as the effects of thermal considerations of all solid body domains on the pump fluid dynamics, frictional losses, leakages, and efficiency behaviors. A set of isothermal and thermal cases were considered and compared to investigate the significance of thermal effects on a fully coupled, lumped parameter Gerotor model with CFD-defined radial and lateral lubricating interfaces.

Comparative analysis of these models shows that the average volumetric efficiency is higher in the thermal model, but the overall hydromechanical efficiency is much lower in the same model when compared to an isothermal model. As such, the total efficiency and the corresponding power loss in the unit for a thermal and isothermal model are similar, indicating that, while the overall efficiency of the Gerotor unit can be approximated with an isothermal model, the individual frictional and leakage losses are sufficiently disparate to warrant the use of a thermal model to more accurately account for volumetric and frictional losses.

For future work, the thermal model will be used for design optimization purposes to maximize the total efficiency of the Gerotor unit.

Nomenclature

Designation	Denotation	Unit
	Symbols	
α_{relax}	Temperature Relaxation Factor	K^{-1}
α_p	Isobaric Expansion Coefficient	K^{-1}
α	Mass Flow Discharge Coefficient	$-$
Δh_{eq}	Deformation Film Height	m
$[H]$	Influence Matrix Operator	$m \cdot Pa^{-1}$
p	Pressure	Pa
T	Temperature	K
K_T	Bulk Modulus	Pa
$\dot{m}_i$	Mass Flow Rate	kg/s
c_p	Specific Heat Capacity	$JK^{-1}kg^{-1}$
ρ	Density	kg/m^3
h	Fluid Film Thickness	m
h_t	Tooth Tip Gap	m
b	Face Width	m
ω	Angular Velocity	$rad \cdot s^{-1}$
r	Radius	m
μ	Fluid Viscosity	$Pa \cdot s$
R_{eq}	Root Mean Square Roughness	m
ϕ_P	Pressure Flow Factor	$-$
ϕ_c	Contact Flow Factor	$-$
ϕ_s	Shear Flow Factor	$-$
ϕ_R	Roughness Flow Factor	$-$
ϕ_D	Energy Dissipation	J/m^3
μ_{Asp}	Asperity Friction Coefficient	$-$
p_{Cont}	Contact Pressure	Pa
$\vec{v}_m$	Mean Surface Velocity	m/s
$\vec{v}_t$	Top Surface Velocity	m/s
$\vec{v}_b$	Bottom Surface Velocity	m/s
$\vec{v}_D$	Relative Surface Velocity	m/s
λ_f	Fluid Thermal Conductivity	$W/m/K$
λ_S	Solid Thermal Conductivity	$W/m/K$
ϵ_T	Thermal Strain	$-$
ϵ	Strain	$-$
f	Constraint Force per Unit Volume	N/m^3
μ_L, λ_L	Lame's Parameters	Pa
ν	Poisson's Ratio	$-$
E	Elastic Young's Modulus	Pa
Ω_S	Surface Area of Influence	m^2
$[C]$	Legendre Polynomial Matrix	$-$
Q_{outlet}	Actual Volume Flow Rate	m^3/s
Δp	Difference between Inlet & Outlet Port Pressure	Pa
T_{shaft}	Shaft Torque	Nm
T_{inner}	Inner Gear Torque	Nm
T_{outer}	Outer Gear Torque	Nm
$Q_{loss,thermal}$	Isothermal Simulation Volumetric Flow Loss	m^3/s
$Q_{loss,isothermal}$	Thermal Simulation Volumetric Flow Loss	m^3/s
η_{vol}	Volumetric Efficiency	%
η_{hm}	Hydromechanical Efficiency	%
η_{total}	Total Efficiency	%
P_{loss}	Percentage of Power Loss	%

Abbreviations	
LP	Lumped Parameter
TSVs	Tooth Space Volumes
PDMs	Positive Displacement Machines
EGM	External Gear Machine
CIGP	Crescent-type Internal Gear Pumps
CFD	Computational Fluid Dynamics
EHL	Elasto-Hydrodynamic Lubrication
TEHL	Thermo-Elastohydrodynamic Lubrication
CVs	Control Volumes
FSI	Fluid Structure Interaction
IM	Influence Matrix
Re	Reynolds Number
LPCM	Lobatto Point Collocation Method
DOFs	Degree of Freedom
FEM	Finite Element Method

References

[1] Kammerl, L., Dautry, E., & Kretzer, C. (2025, February 20). Gerotor Pump And Motor/Pump Unit.

[2] Thiagarajan, D., & Vacca, A. (2014), "A Numerical Procedure to Design the Optimal Axial Balance of Pressure Compensated Gear Machines," 8th FPNI Ph. D Symposium on Fluid Power, Lappeenranta, Finland.

[3] Thiagarajan, D., Dhar, S., & Vacca, A. (2015), "A novel fluid structure interaction-EHD model and optimization procedure for an asymmetrical axially balanced external gear machine," Tribology Transactions, 58(2), 274-287.

[4] R. Pippes, C.Mayer., (2002), "Gap-compensated high-pressure internal gear pumps", 3rd International Fluid Power Conference, Volume 2, pp.203. IFK3, 2002, Aachen, Germany.

[5] Pan, D., Vacca, A., (2023), "Total efficiency prediction of crescent-type internal gear pump considering floating balancing components", ASME/BATH 2023 Symposium on Fluid Power and Motion Control.

[6] Manco, S., Nervegna, N., Rundo, M., Armenio, G., Pachetti, C., and Trichilo, R., 1998, "Gerotor Lubricating Oil Pump for IC Engines," SAE Trans., 107(3), pp. 2267–2283.

[7] Gamez-Montero, P. J., Castilla, R., Del Campo, D., Ert€urk, N., Raush, G., Codina, E., (2012), "Influence of the Interteeth Clearances on the Flow Ripple in a Gerotor Pump for Engine Lubrication," Proc. Inst. Mech. Eng., Part D, 226(7), pp. 930–942.

[8] Castilla, R., Gamez-Montero, P. J., Raush, G., Codina, E., (2017), "Method for Fluid Flow Simulation of a Gerotor Pump Using OpenFOAM," ASME J. Fluids Eng., 139(11), p. 111101.

[9] Altare, G., Rundo, M., (2016), "Computational Fluid Dynamics Analysis of Gerotor Lubricating Pumps at High-Speed: Geometric Features Influencing the Filling Capability," ASME J. Fluids Eng., 138(11), p. 111101.

[10] Bae, J. H., Kwak, H. S., San, S., Kim, C., 2016, "Design and CFD Analysis of Gerotor with Multiple Profiles (Ellipse–Involute–Ellipse Type and 3-Ellipses Type) Using Rotation and Translation Algorithm," Proc. Inst. Mech. Eng., Part C, 230(5), pp. 804–823.

[11] Pellegri, M., Vacca, A., Devendran, R. S., Dautry, E., and Ginsberg, B., 2016, "A Lumped Parameter Approach for GEROTOR Pumps: Model Formulation and Experimental Validation," Tenth International Fluid Power Conference, Dresden, Germany, Mar. 8–10.

[12] Pellegri, M., and Vacca, A., 2017, "Numerical Simulation of Gerotor Pumps Considering Rotor Micro-Motions," Meccanica, 52(8), pp. 1851–1870.

[13] Pellegri, M., (2018), "A Study on the Operation of Gerotor Type Units Considering Fluid Structure and Mechanical Interaction Effects", (dissertation).

[14] Mistry, Z., Manne, V., Vacca, A., Dautry, E., Petzold, M., 2020, "A Numerical Model for the Evaluation of Gerotor Torque Considering Multiple Contact Points and Fluid-Structure Interactions," Volume 1 – Symposium, 409–418.

[15] M. Ivantysynova (at that time Berge), "An investigation of viscous flow in lubricating gaps. (In Slovak)," SVST Bratislava, Czechoslovakia, 1983.

[16] Rituraj, R., Vacca, A., & Morselli, M. A. (2020), "Thermal modelling of external gear machines and experimental validation.", Energies, 13(11), 2920.

[17] Mukherjee, S., Shang, L., Vacca, A., "A Fast Approach for Coupled Fluid-Thermal Modelling of the Lubricating Interfaces of Axial Piston Machines," Volume 1 - Symposium, 327–340.

[18] Mukherjee, S., Shang, L., Vacca, A., "Numerical analysis and experimental validation of the coupled thermal effects in swashplate type axial piston machines," Mechanical Systems and Signal Processing, 220, 111673.

[19] Pawar, A., Vacca, A., Rigosi M., (2024), "Comparative Analysis of External Gear Machine Performance Considering Deformation and Thermal Effects".

[20] Manne, V. H., Vacca, A., & Singh, K. (2023). A curve-fit traction coefficient relation of mixed EHL line contact

with hydraulic fluid and steel surfaces. *Tribology Transactions*, *66*(2), 364–380. https://doi.org/10.1080/10402004.2022.2163947

[21] Rituraj F, Vacca A., (2019), "Modelling and Validation of Tooth Tip Leakages in Gerotor Pumps," Proceedings of the ASME-JSME-KSME 2019 Joint Fluids Engineering Conference AJKFLUIDS

[22] Ransegnola, T., Zappaterra, F., Vacca, A., (2022), "A Strongly Coupled Simulation Model for External Gear Machines Considering Fluid-Structure Induced Cavitation and Mixed Lubrication," Applied Mathematical Modelling, 104, 721–749.

[23] Mukherjee, S., Vacca, A., Shang, L., Sharma, A., (2023), "A thermal modeling approach for the piston/cylinder interface of an axial piston machine under asperity contact," Meccanica 58 (10) 1929–1957.

[24] Lee, S. C., Ren, N., (1996) "Behavior of Elastic-Plastic rough surface contacts as affected by surface topography, load, and material hardness.", Tribology Transactions, 39(1), 67–74.

[25] Elrod H.G., Brewe E., (1991) "Efficient numerical method for computation of the thermohydrodynamics of laminar lubricating films", Tribol. 113 (3) 506–511.

[26] Zhang S., Hassini M.A., Arghir M., (2018) "Accuracy and grid convergence of the numerical solution of the energy equation in fluid film lubrication: Application to the 1D slider", Lubricants 6 (4).

[27] Zecchi, M. (2013). (dissertation). A novel fluid structure interaction and thermal model to predict the cylinder block.